HHS Public Access

Author manuscript

Nat Neurosci. Author manuscript; available in PMC 2015 February 13.

Published in final edited form as:

Nat Neurosci. 2014 July ; 17(7): 953–961. doi:10.1038/nn.3738.

Functional organization of glomerular maps in the mouse accessory olfactory bulb

Gary F. Hammen[1], **Diwakar Turaga**[1], **Timothy E. Holy**[1,*], and **Julian P. Meeks**[2,*]

[1]Washington University School of Medicine, St. Louis, MO

[2]The University of Texas Southwestern Medical Center, Dallas, TX

Summary

The mammalian accessory olfactory system (AOS) extracts information about species, sex, and individual identity from social odors, but its functional organization remains unclear. We imaged presynaptic Ca^{2+} signals in vomeronasal inputs to the accessory olfactory bulb (AOB) during peripheral stimulation using light sheet microscopy. Urine- and steroid-responsive glomeruli densely innervated the anterior AOB. Glomerular activity maps for sexually mature female mouse urine overlapped maps for juvenile and/or gonadectomized urine of both sexes, whereas maps for sexually mature male urine were highly distinct. Further spatial analysis revealed a complicated organization involving selective juxtaposition and dispersal of functionally-grouped glomerular classes. Glomeruli that were similarly tuned to urines were often closely associated, whereas more disparately tuned glomeruli were selectively dispersed. Maps to a panel of sulfated steroid odorants identified tightly-juxtaposed groups that were disparately tuned and dispersed groups that were similarly tuned. These results reveal a modular, non-chemotopic spatial organization in the AOB.

Neural circuits decode the sensory world through a highly refined series of synaptic connections. Because most neuronal circuitry is local, progress in dissecting functional interactions has long emphasized the nervous system's spatial organization[1-6]. Indeed, discovering how sensory modalities are "mapped" to regions of the brain was an essential step in deciphering their function. Discoveries in the visual and somatosensory cortices revealed links between sensory parameters and the location of neural responses, indicating that these sensory systems possessed "topographic maps"[1, 2]. Whether topographic or non-topographic, sensory maps have served as a foundation for our understanding of the brain.

However, many regions of the brain do not have a natural correspondence to external space; there is considerable interest in understanding the principles of spatial organization that govern such circuits. In the chemical senses, one prominent form of spatial organization is observed in the olfactory bulb, in which olfactory sensory neurons expressing the same

*These authors contributed equally to this work.

A supplementary methods checklist is available.

The authors report no conflicts of interest.

receptor gene project their axons into common regions of neuropil called "glomeruli"[4, 7]. This organization pools the output of many individual sensory neurons with identical specificity for odorants. This glomerular organization serves as a form of sensory map, since particular functional responses are reproducibly localized to particular regions[8]. In the main olfactory bulb (MOB) of rodents, numerous studies have defined the position and tuning profiles of many of the glomeruli[6, 9-17]. While this map is reproducible across animals, no overarching principle has been discovered that broadly describes its spatial organization[18]. The lack of a cohesive model for MOB topography might be a consequence of the huge diversity of odorous compounds and difficulties inherent in determining how "proximity in chemical space" is related to odorant receptor structure and axon targeting.

To overcome these barriers, one promising approach is to study maps and topography in an olfactory system selective for a narrower range of stimuli. An attractive candidate is the accessory olfactory system (AOS), also called the vomeronasal system, which specializes in the detection of social odors[19]. Vomeronasal sensory neurons (VSNs), neuroepithelial cells in the vomeronasal organ (VNO) project axons to the first AOS circuit, the accessory olfactory bulb (AOB). The AOB receives all of its synaptic inputs within a densely packed glomerular layer. In mice, this layer covers less than a square millimeter of the brain surface and is roughly 150 μm deep, in principle allowing optical observation of nearly all synaptic inputs into the AOB in a single experiment. An important difference between the AOB and the MOB is that VSNs expressing the same receptor gene (members of a "VSN type") target multiple AOB glomeruli, and do so with significant variability across experimental subjects[20, 21]. Until now, the only studies of the organization of the glomerular layer have been anatomical, in which one[20, 21] or a few[22] VSN types were tagged with a fluorescent label. Such studies provide a precise but narrow snapshot of the organization of AOB inputs. Moreover, because the molecules that activated VSN types were unknown, the relationships between glomerular receptive fields and physical positions have remained unexplored.

However, any attempt to determine the functional organization of the AOB must address a number of technical obstacles. AOB glomeruli are small (10–80 μm in diameter), variable in shape, and stacked on top of one another in depth, so obtaining an exhaustive functional map requires methods to quickly image activity in three dimensions throughout large volumes. We combined *ex vivo* methods that expose the AOB surface[23] with calcium imaging via objective-coupled planar illumination (OCPI) microscopy[24]. By stimulating VSNs with AOS odorants, including urine from different developmental stages and sulfated steroids[25], we obtained the first large-scale functional images of the AOB glomerular layer. Our results identify organizational features across spatial scales, and reveal a modular organization in this circuit that physically juxtaposes certain inputs and selectively disperses others.

Results

We studied AOBs from adult male transgenic mice expressing the Ca^{2+}-sensitive fluorescent protein GCaMP2 in the cytoplasm of VSNs[26]. We imaged GCaMP2 fluorescence in the glomerular layer of the AOB while stimulating peripheral VSNs with mouse urine and sulfated steroids in live *ex vivo* preparations of the AOS[27] (Fig. 1a). Image stack dimensions were approximately 700 μm along both the anterior-posterior and medial-

lateral axes and nearly 200 μm deep into the tissue (Fig. 1b). These image stacks encompassed the entire anterior AOB (aAOB) and approximately 1/3 of the posterior AOB (pAOB, Fig. 1b, Supplementary Movie 1) and were acquired every 5 seconds while stimuli were delivered to the VNO. Responses were recorded continuously for periods up to an hour and forty minutes.

Sex-specific glomerular maps are activated by mouse urine

We hypothesized that male- or female-responsive glomeruli might occupy specific spatial domains within the aAOB. Previous electrophysiological recordings identified aAOB mitral cells responding to dilute male and female urine, without clear evidence of sex-dependent spatial organization[28]. However, mitral cells possess extensive dendritic arbors with connections to multiple glomeruli spanning large distances[22, 29, 30], which might complicate understanding of local circuits. We observed fluorescence intensity changes in the glomerular layer when we stimulated the VNO with 100-fold dilute adult, sexually-naïve BALB/c female and male mouse urine, but not with Ringer's control saline (Fig. 1c). As in previous studies of male- and female-selective neural responses, we pooled urine from many individual mice in order to stimulate sex-specific responses that represent the "average" of each sex. We calculated a response reliability index (*RRI*, which reports signal-to-noise ratio) for each image voxel by normalizing the fluorescence changes to the across-trial noise (Fig. 1d). We used *RRI* values to identify regions of interest (ROIs) representing putative glomeruli. These glomerular ROIs showed stimulus-dependent increases in fluorescence, consistent with previous Ca^{2+} imaging from VSNs[26, 31] (Fig. 1e). In the AOB, glomerular boundaries are often poorly-defined by anatomical criteria[20], but when visible these boundaries aligned well with activated ROIs (Fig. 1f). Moreover, GCaMP2 activation highlighted regions that could not be distinguished based on morphological cues alone (Fig. 1f).

To compare male and female urine-responsive glomerular maps, we aligned AOBs to visual boundaries in each image (Fig. 2; see Methods). Consistent with previous reports[24], we observed strong aAOB responses to 1:100 BALB/c female urine (Fig. 2a). The sum volume of all glomeruli activated by 1:100 BALB/c female urine was 4-fold larger than was activated by 1:100 BALB/c male urine (4.4 ± 1.6 fold, n = 8, p = 0.043, Fig. 2a, b). A much larger fraction of male urine-responsive than female urine-responsive voxels were located in the visible regions of the pAOB (32 ± 8% male versus 2 ± 1% female; p = 0.007; n = 8; Fig. 2b). Female urine-responsive ROIs tended to be larger than male urine-responsive ROIs (Fig. 2c, p = 0.032 Kolmogorov-Smirnoff test). Because ROI volumes increase with the intensity of the $\Delta F/F$ response, this effect may be influenced by stronger maximal activation by BALB/c female urine than male urine, but might also suggest that female urine-responsive glomeruli possess a larger synaptic territory in the AOB.

We observed a small but significant number of ROIs that responded to both male and female urine (Fig. 2a, d). To ensure that this effect was not due to inclusion of very weak responses to male urine, we evaluated glomerular ROI responses at multiple thresholds. The overlap persisted until very high thresholds, confirming that these glomerular ROIs were activated by cues found in both male and female urine (constituting 4 ± 3% of female and 9 ± 4 % of

male urine responsive voxels at $\Delta F/F > 2\%$, n = 8, Fig. 2d). This population represented a larger fraction of the male urine-responsive ROIs, owing largely to the larger overall pool of female-responsive ROIs.

Glomerular maps encode both sex and maturity from urine

If the only function of the AOS were to distinguish sex, one might naturally wonder why so many glomeruli respond to female urinary cues. The four-fold difference in overall volume of the AOB glomerular layer activated by male and female urine mirrors observed differences in the number of VSNs demonstrating sex selectivity for urine[24]. Given that a small number of sex-selective VSNs and AOB neurons is theoretically sufficient for sex classification[32], we hypothesized that some of the abundant female urine-selective glomeruli may encode biologically-relevant features other than sex, for example sexual maturity[26]. We therefore compared glomerular activity maps generated by VNO stimulation with juvenile (P21), gonadectomized, and sexually mature urine from the same BALB/c mouse strain.

Each of these 6 urinary cues activated at least one glomerulus (Fig. 3). Glomerular maps generated by this stimulus set revealed the rich combinatorial nature of responses in the AOB (Fig. 3a–c). Many of the glomeruli demonstrated selectivity for certain urines, indicated by an increase the numbers of selective ROIs and a decrease in the number of non-selective ROIs at higher $\Delta F/F$ thresholds (Fig. 3d). The large majority of ROIs activated by sexually mature female urine also responded to juvenile and/or gonadectomized urine of one or both sexes (86 ± 3% at $\Delta F/F > 2\%$, n = 5; Fig. 3a, c, e). Thus, only a small fraction of the female urine-responsive aAOB glomeruli are exclusively tuned, or “selective,” for urine from adult intact females at this concentration (Fig. 3e). This was not the case for male urine-responsive glomeruli, which showed almost no overlap between intact, juvenile, and castrated males (Fig. 3b). Including all stimuli, we found that the large majority of intact male urine-responsive ROIs were also selective for this stimulus (70 ± 14%, $p < 0.05$ one-way ANOVA, n = 5, Fig. 3e). Intact adult female urine responses were nearly entirely abolished by sulfatase treatment (Supplementary Fig. 1), confirming that sulfated compounds dominate the AOS activity induced by female urine[25].

Evaluation of all urine responses revealed specific, repeated tuning patterns among aAOB glomeruli (Fig. 3f). Clusters displayed responsivity for anywhere from one to five of the six stimuli, with approximately half of the ROIs dominated by one or two stimuli. This classification of glomeruli into types serves as a foundation for analysis of the spatial organization of responses to natural stimuli (Fig. 3g, Supplementary Fig. 1).

Sets of functionally-defined glomeruli form spatial modules

Because the AOB’s evaluation and analysis of natural stimuli might be based on local circuitry, we wondered whether glomeruli exhibited patterns in the relationship between their receptive fields (Fig. 3f) and their spatial organization (Fig. 3g). To evaluate such questions statistically, we compared the observed positional patterns against those that arose from randomly shuffling the cluster label assigned to each ROI.

Several glomerular clusters were preferentially spatially distributed along the 3 orthogonal axes (Fig. 4a–b, Supplementary Fig. 1). Intact adult female urine-selective glomeruli (Cluster 1) were preferentially located near the anterior tip of the AOB ($p < 0.05$, $n = 5$, Fig. 4b). In contrast, intact adult male urine-selective glomeruli (Cluster 2) were preferentially located more posteriorly, very near the *linea alba* dividing the aAOB and pAOB ($p < 0.05$, $n = 5$, Fig. 4b). Cluster 3 glomeruli were preferentially located approximately mid-way between Clusters 1 and 2 along the anterior/posterior axis ($p < 0.05$, $n = 5$, Fig. 4b). Cluster 1 glomeruli were frequently among the most medial of all activated glomeruli, and had an unusually-strong tendency to be superficial rather than deep ($p < 0.05$, $n = 5$, Fig. 4b). Cluster 3 glomeruli were biased towards deeper positions ($p < 0.05$, $n = 5$, Fig. 4b).

In addition to the regularities in absolute positioning exhibited by three of these clusters, we asked whether there might be reproducible patterns in the relative positioning between two or more clusters[22]. Again using comparisons against shuffled maps(Fig. 4 c–f), we found that the largest effects consisted of dispersals: for example, Cluster 1 ROIs (selective for intact adult female urine) and Cluster 4 ROIs (selective for juvenile urine) were much farther apart than expected by chance (Fig. 4c, d; $p < 1e^{-7}$, $n = 5$). A similar result held for Clusters 1 and 2 ($p < 1e^{-7}$), Clusters 4 and 5 ($p < 1e^{-3}$), and Clusters 4 and 6 ($p < 1e^{-8}$; all $n = 5$, Fig. 4d–f). We also found 2 clear instances of preferentially-juxtaposed functional groups (Fig. 4d–f). Cluster 3 (responsive to intact adult female and juvenile urine) and Cluster 4 (responsive to juvenile urine only) tended to be near one another (Fig. 4d–f, $p < 0.01$, $n = 5$). Likewise Cluster 5 (responsive to all female urines and juvenile male urine) and Cluster 6 (responsive to all urines except intact adult male urine) tended to be closer than expected by chance ($p < 0.01$, Fig. 4d–f). Clusters 1 and 2, selective for intact adult female urine and intact adult male urine, only showed preferential dispersal with other groups. Clusters 4, 5, and 6 showed preferential juxtaposition in some pairwise comparisons and preferential dispersal in others.

In both cases of selective juxtaposition, the glomeruli were similarly tuned, with the two members of each pair differing by only one response. Selectively dispersed groups, on the other hand, were more dissimilarly tuned (*i.e.* differing by at least 2 responses). At face value, this suggested that relative spacing among glomeruli may selectively group similarly-tuned inputs and disperse dissimilarly-tuned inputs. Such an organization would suggest that the AOB possesses “identity-based” chemotopy based on relative glomerular position. However, because the blend of odorants in each urine source is unknown, it remains unclear from these data whether preferential juxtaposition and dispersal among glomeruli reflects sensitivity to similar molecules.

Steroid-responsive glomeruli span the aAOB and pAOB

To make explicit comparisons between glomerular spatial organization and odorant chemical structures, we generated maps to a panel of 11 synthetic sulfated steroids, a prominent class of natural ligands[25]. This panel of sulfated steroids, spanning the androgen, estrogen, pregnanolone, and glucocorticoid families, was delivered at 10 μM, a concentration previously found to activate at least 10 functionally-separable VSN populations[27, 31]. Across 10 adult experimental subjects, we identified 1078 glomeruli that

responded to at least one of the 11 synthetic sulfated steroids with Δ*F*/*F* greater than 1%. We observed reliable, concentration-dependent glomerular activity across multiple stimulus trials (Fig. 5a–b, Supplementary Fig. 2, and Supplementary Movie 2). Within glomerular regions of interest (ROIs), fluorescence peaked within the first image stack (within 5 s), and then accommodated over subsequent image stacks (Fig. 5b). Single-plane imaging at 10 Hz indicated that fluorescence increases began within 1–2 s of stimulus onset, and peaked within 3–5 s (Supplementary Fig. 2, Supplementary Movie 3). The vast majority (1012 of 1078, 94%, Δ*F*/*F* > 1%, n = 10) of steroid-responsive ROIs were located in the aAOB, but were widely distributed within this subregion (Fig. 5c–f, Supplementary Fig. 3, Supplementary Movie 4). Since V1R-expressing VSNs selectively innervate the aAOB[20, 21], these results confirm that many VSNs expressing V1Rs are sensitive to sulfated steroids[31, 33].

We observed a notable number of glomeruli responsive to sulfated pregnanolones in the posterior AOB (56 of 576 pregnan-responsive glomeruli, representing 85% of all posterior responses). These glomeruli likely derive from a pregnanolone-responsive population of basal VSNs[31]. We further investigated this pAOB activity by comparing activity maps at different sulfated steroid concentrations (Supplementary Fig. 2). We found reliable aAOB responses to most of the sulfated steroids in the panel starting at 1 μM (Supplementary Fig. 2), consistent with previous results[25, 34]. Glomeruli responsive to allopregnanolone sulfate (P3817) were found in the pAOB at 10 μM (Supplementary Fig. 2). At 100 μM, activity in the pAOB increased markedly to another sulfated pregnanolone, P8200, but less so to other sulfated steroids (Supplementary Fig. 2). Since the pAOB receives input from V2R-expressing VSNs, these results suggest that sulfated pregnanolones elicit activity in both major vomeronasal receptor families.

Because sulfated steroid abundance is high in BALB/c female urine[25], we investigated spatial relationships between synthetic steroid ROIs and female urine-responsive ROIs. We observed many glomerular ROIs that were activated by both 10 μM Q1570 and 1:100 intact adult BALB/c female urine, consistent with previous results[25, 35] (Supplementary Fig. 4). We also observed many glomeruli that responded to both 10 μM epitestosterone sulfate (A6940) and 1:100 BALB/c female urine (Supplementary Fig. 4), suggesting that female urine contains odorants that activate the same inputs as certain sulfated androgens. Glucocorticoid overlap was also seen for juvenile male and female and ovariectomized female urine (Supplementary Fig. 4), suggesting these glucocorticoids are present at comparable concentrations in these urine sources. Also apparent in this comparison was the low incidence of overlap between these sulfated steroids and intact adult male urine (*e.g.* Q1570 overlap was 7 ± 1% for female urine and 0 ± 0.1% for male urine, $p < 0.05$ Kruskal-Wallis test, n = 7, Supplementary Fig. 4).

Glomerular juxtaposition does not infer similar tuning

To determine whether individual glomeruli are organized by their tuning for molecular features, we first analyzed the glomerular activity patterns to synthetic sulfated using clustering algorithms[27, 31]. We found that glomerular responses to these steroids fell into at least 10 classes of reproducible patterns (Fig. 6a–c). These classes match previous

physiological recordings in VSNs[27, 31], and nearly every glomerulus (1071/1078, 99%) could be assigned to one of these classes. Cluster features remained consistent across response thresholds (Supplementary Fig. 5). This suggests that glomerular responses to sulfated steroids reflect these functionally-defined peripheral populations.

To compare receptive fields to molecular features of the ligands (Fig. 7a), we calculated 1,666 molecular descriptors[36] for each sulfated steroid in the panel, then computed the average pairwise Euclidean distance between the normalized odorant descriptors sensed by each VSN class. This produced quantitative measurements of receptive field differences between all VSN classes (Fig. 7b). The distinctions among most VSN response classes had a clear corresponding structural basis – compounds with similar molecular features were more likely to co-activate the same glomerulus –but some classes showed selectivity for steroids differing in subtle aspects poorly captured by these descriptors (*e.g.*, the 3 sulfated pregnanolones).

The absolute glomerular positions for most VSN classes showed no evidence of selective positioning along the 3 orthogonal axes. The exceptions were a strong posterior bias among Class 5 glomeruli, selective for allopregnanolone sulfate (P3817), and a bias among Class 7 glomeruli (selective for 17β-estradiol disulfate) to lie laterally along the *linea alba* (Supplementary Fig. 6). Visual inspection of activity maps for similarly tuned VSN classes revealed no evidence of a positive link between physical closeness and receptive field similarity (Fig. 7c). For example, the three pregnanolone-responsive classes had highly similar receptive fields, but were not similar in their projection patterns (Fig. 7b–c). At face value, these data indicate that at fine spatial scales, VSNs sensing highly similar odorants do not necessarily project to physically adjacent locations.

We next sought to determine whether any of these functionally-defined classes showed evidence of higher-order spatial relationships. We compared pairwise distances between the 45 combinations of VSN class pairs, and identified two tightly juxtaposed pairs. The most tightly juxtaposed pair was Class 4 – 8 ($p < 1e^{-5}$, Fig. 8a; Supplementary Movie 4). The second pair was Class 6 – 10 ($p < 0.01$, $n = 10$). As was the case for our investigation of spatial similarity among urine-responsive glomeruli (Fig. 4), we observed glomeruli for many VSN class pairs (14 total) that were preferentially dispersed compared to shuffle test expectations ($p < 0.05$, $n = 10$, Fig. 8b). In all, 16 of the 45 VSN class pairs (36%) showed a reciprocal statistically significant spatial relationship (Fig. 8b). We also observed several non-reciprocal significant spatial relationships (for example, Class 1 – 3, Fig. 8b), indicating tight juxtaposition between subsets of glomeruli in certain class pairs.

The juxtaposed glomeruli in the Class 4 – 8 pair arose from VSN classes with the most distant receptive fields in our analysis (Fig 8c–d). The Class 6 – 10 pair did not possess strongly similar or dissimilar receptive fields compared to other pairs (Fig. 8c–d). Among the most spatially dispersed pairs was Class 3–5, sensitive to pregnanolone stereoisomers, the most molecularly-similar ligands in our stimulus set (Fig. 7a, c). To test whether there was a consistent relationship between glomerular receptive fields and relative spacing, we generated a spring embedding model in which receptive field similarity was used as the spring constant and spatial similarity was used for the distance between points (Fig. 8d). The

model energy necessary to produce the observed isomap (*i.e*. the product of spatial distance and the spring constant) was near the mean values expected from shuffled maps (observed energy 7.1, Gaussian fit of shuffle test: $\mu = 6.8$, $\sigma = 0.8$, $p = 0.63$). This indicates that, in aggregate, the preferential juxtaposition and dispersal of AOB glomeruli is not organized by the similarity or dissimilarity of their odorant tuning.

Discussion

A distributed glomerular code for sex and maturity

Many individual VSNs and AOB mitral cells are selective for the sex, strain, and species of urine sources[26-28, 32, 37-39]. Several studies have demonstrated that the aAOB and pAOB become strongly active during exposure to female or male urinary cues, respectively[40, 41]. However, male urine also has been shown to activate the aAOB, and female urine in the pAOB[24, 41], suggesting that each of these major AOB subregions possess the capacity to compare sex-selective signals. The majority of AOB glomerular responses to VNO stimulation with 100-fold diluted mouse urine of both sexes were located in the aAOB, suggesting that, at these concentrations, this V1R-receptive AOB region is a prominent site of sex discrimination.

We compared activity patterns induced by intact adult urine to those generated by urine of sexually immature or gonadectomized animals. This combinatorial approach revealed that only 14% of the ROIs that respond strongly to intact BALB/c female urine responded exclusively to this urine type, with the most prominent sources of overlap being juvenile urine of either sex. Thus, the odorants present in sexually mature BALB/c female urine activate VRs that are also sensitive to odorants in sexually immature urine. These broadly responsive inputs are poor candidates for performing discriminations that underlie specific behavioral responses to sexually mature adult females, and may instead be involved in multi-glomerular comparisons between non-male individuals. Glomeruli selective for sexually mature female urine were preferentially located along the anterior aAOB border and at superficial depths.

Glomeruli selective for sexually-mature male urine were preferentially located near the posterior edge of the aAOB near the *linea alba*. Many fewer ROIs responded to intact adult male urine, but most (70%) of these ROIs were exclusively activated by it. As such, the activity generated by the AOS in response to mature male urine appears to be more directly indicative of a sexually intact BALB/c male. This also indicates that sexually mature males, but not juvenile or gonadectomized males, cease producing urinary odorants common to sexually mature female mice. This implies that changes in metabolic pathways in intact males result in halted production, metabolic shunting, or accelerated degradation of many AOS odorants.

Our combinatorial approach to studying AOB glomerular maps also revealed that juvenile female and male urine were the most potent sources of aAOB activators in our study, activating nearly two-fold more glomerular ROIs than even intact BALB/c female urine. Nearly one-third of these ROIs were exclusively activated by both juvenile male and female urine. Discovery of this population suggests a large number of inputs to the aAOB possess

the capacity to discriminate sexually immature animals at weaning age (P21) from sexually mature adults. These inputs are prime candidates for guiding behaviors towards these young animals.

Juxtaposed glomeruli have correlated urine tuning

To date, the clearest indication that the AOB glomerular layer possesses a systematic organization at fine scales came from anatomical studies labeling two or more members of the same "clade"[22]. In these studies, VSNs types in the same clade were found to closely appose their glomeruli[22]. Because clade definitions were based on amino acid homology for the entire receptor, this result suggested a modular glomerular organization that juxtaposes inputs with similar receptive properties. We measured the pairwise distances between glomeruli with different receptive fields for sexually mature and immature urines, and found strong evidence for preferential juxtaposition among two of these glomerular populations. We also found evidence for strong preferential dispersal among other glomerular populations. These findings suggest that relative spacing between glomerular populations may be a prominent "axis" upon which biologically-relevant spatial relationships might be built in the AOB.

The preferentially juxtaposed glomerular groups all responded to juvenile urine of both sexes but differed in their sensitivities to various adult urines. Each of these juxtaposed pairs differed only by sensitivity to just one of these stimuli, whereas each of the preferentially dispersed glomeruli differed by more than one. At face value, this might seem to suggest that preferential glomerular juxtaposition is associated with similar organismal status, which would constitute a form of chemotopy. However, the urinary odorants activating juxtaposed glomeruli may or may not be molecularly similar. To address this question, we performed similar experiments using a defined panel of sulfated steroid odorants known to activate distinguishable VSN populations[27, 31].

Sulfated steroids activate aAOB and pAOB glomeruli

At the most macroscopic scale, the AOB has a tripartite organization determined by innervation of VSNs expressing receptors from different families[42]. However, how these macroscopic regions correspond to receptivity to defined ligands has scarcely been explored. The 11 synthetic sulfated steroids were chosen to match previously-identified functional groups of similarly-tuned VSNs[27, 31]. The breadth of our stimuli allowed us to compare glomerular activation patterns to chemically similar and distinct odorants. AOB glomerular responses to sulfated steroids showed concentration dependence, with sensitivity to some sulfated steroids at 1 μM. AOB responses to steroids at 1 to 10 μM showed increased peak fluorescence within glomeruli but few changes in the macroscopic activity pattern. This was in stark contrast to the responses at 100 μM, which dramatically changed both the intensity and number of activated glomeruli. At 100 μM, activated glomeruli retained some stimulus specificity, consistent with previous reports[25, 33], and indicating that even at 100 μM sulfated steroids do not gate a nonspecific conductance in VSNs.

The physical location of steroid-responsive glomeruli was dispersed across the aAOB. This is consistent with previous observations that sulfated steroids activate apical[31] and V1R-

expressing VSNs[33]. The small (6%) but consistent population of steroid-responsive glomeruli in the pAOB were dominated by glomeruli responding to certain sulfated pregnanolones. This posterior activity was strongly concentration-dependent, but was present in some cases even at 1 μM, suggesting either a displaced V1R-expressing population projects to the pAOB, or that some VSNs expressing V2Rs are sensitive to sulfated pregnanolones.

The glomerular activity patterns across the panel of 11 synthetic sulfated steroids, matched those previously observed in VSNs using multielectrode array recordings[27], and population calcium imaging[31]. This suggests that our experimental setup was capable of accurately producing topographical maps in the AOB downstream of functionally-defined sets of VSNs. Some glomerular ROIs assigned to functional classes possessed lower-intensity activity patterns that resembled those of other classes (see Fig. 6b). These particular ROIs may encompass parts of two anatomical glomeruli.

Glomerular proximity is not based on odorant similarity

In chemical senses, regional specificities are apparent, but scarce evidence of systematic positional relationships between these regions has been found[18]; however, this question has never been considered for the AOB, which is activated by a narrower range of stimuli. We explored the hypothesis that systematically juxtaposed glomeruli have similar receptive fields. Similarly-tuned glomeruli were not always found in tightly-packed groups. This was especially evident for Classes 3–5, responsive to pregnanolone stereoisomers, which showed preferential dispersal rather than juxtaposition. Additionally, the most preferentially juxtaposed pair, Classes 4–8, responded to the most disparate ligands in the study (sulfated pregnanolone and estrogen-selective inputs, respectively). In combination with evidence that receptors within the same clade, at least in some circumstances, target neighboring glomeruli[22], one possible interpretation of this result is that receptor amino acid sequence is more directly related to axonal targeting than to ligand binding. It is worth noting that our functional clustering scheme may lump multiple, similarly-tuned VSN types together. As such, it may be the case that some ROIs correspond to a clump of indistinguishably-tuned glomeruli. Our results do not suggest that tight glomerular apposition cannot exist between similarly-tuned VSN types, but rather that strong, reproducible juxtaposition does not require similar odorant tuning.

These observations comprise the first clear examples of functionally-defined AOB glomerular “modules,” and demonstrate that the individual glomeruli in these modules can be tuned to odorants with very different molecular features. The apparent discrepancy between juxtaposition and receptive field similarity when evaluating urine-stimulated maps and steroid-stimulated maps may indicate that the organizational principle in the AOB is based on phenotypic, and not molecular, similarity between odorants. This would perhaps indicate that only biologically-significant odorant combinations are selectively juxtaposed in the AOB. The computational benefits of juxtaposing these particular glomeruli remain to be elucidated. Are these adjacent signals integrated by downstream mitral cells or specifically inhibited by local interneurons? Does physically juxtaposing these inputs enable the AOB to identify specific hormonal or behavioral states? Answering these questions will certainly

improve our understanding of the logic of this important social and reproductive sensory pathway.

Methods

Animals

Driver mice with an *OMP-IRES-tTA* (C57Bl/6 background) transgene were mated with transgenic effector mice harboring a tetracycline transactivator response element and minimal promoter 5' of the coding region for the Ca^{2+} protein GCaMP2[26]. 10 adult (>60 days postnatal) male mice were used as experimental animals, with one AOB imaged per animal. Mice were housed in single-sex cages of no more than 5 animals from weaning until experimental use with *ad libitum* access to food and water. Animals were housed on a standard 12 hour – 12 hour light/dark cycle. All BALB/c mice used for urine collection, including surgically-altered mice, were purchased from The Jackson Laboratory. All animal procedures were approved by the Washington University Animal Studies Committee.

Ex vivo preparations

Ex vivo dissections were performed as described previously[23, 43]. Briefly, mice were deeply anesthetized with isofluorane and rapidly decapitated in ice-cold, oxygenated artificial cerebrospinal fluid (aCSF) containing (in mM) NaCl 125, KCl 2.5, $CaCl_2$ 2, $MgCl_2$ 10, $NaHCO_3$ 25, NaH_2PO_4 1.25, myo-inositol 3, Na-pyruvate 2, Na-ascorbate 0.4, glucose 25. A single hemisphere (typically the right) of the dorsal mouse snout and head, up to and including the olfactory bulb and accessory olfactory bulb, was dissected away from the head, glued with Vetbond (3M, St. Paul, MN, USA) to a small plastic plank, and then adhered with silicon vacuum grease (Dow Corning, Midland, MI) to a dissection chamber. In the dissection chamber, the preparation was superfused rapidly with room temperature (22–25° C) aCSF. The vomeronasal nerves were exposed to the superfusate via a secondary microdissection to remove the septal cartilage. The preparation was moved to a customized tissue imaging chamber, and a 0.0056" inner diameter polyimide cannula was carefully placed inside the vomeronasal organ (VNO) lumen. We delivered a steady stream (0.2 mL/min) of Ringer's saline, into which all stimuli were diluted, to the VNO. At this flow rate, the VNO lumen (approximately 2 μL in volume) was replaced approximately every 0.5–1 s. Ringer's saline contained (in mM) NaCl 115, KCl 5, CaCl2 2, MgCl2 2, NaHCO3 25, HEPES 10, glucose 10.

Stimuli

On the day of the experiment, VNO stimuli were dissolved to their final concentrations (100 nM – 100 μM) in Ringer's solution. Sulfated steroids were purchased from Steraloids, Inc. (Newport, RI, USA) and stock solutions (20–100 mM) produced by dissolving steroids into methanol or filtered, distilled water. The sulfated steroids applied are listed in Table 1.

Although VNO recordings have not demonstrated sensitivity of vomeronasal sensory neurons to methanol at 2,000–10,000-fold dilutions, control Ringer's stimuli (to which other responses were compared) always contained the maximum methanol concentration applied across all stimuli.

BALB/c urine was collected using methods described previously (Nodari et al., 2008). For intact adult male and female urine, single-sex cages of intact adult (>P60) BALB/c male or female mice were suspended in wire-mesh bottom cages above liquid nitrogen. Frozen urine from several cages was pooled across several days' collections, then centrifuged and filtered to remove particulates. Pooling female mouse urine likely incorporated substances found in female urine at various stages of the estrous cycle, and averaged them over time. For juvenile (P21) and gonadectomized mice, urine was collected continuously for 72 hours, and was pooled across 10 animals, housed in two groups of five.

We followed protocols for sulfatase treatment of female urine previously reported[25] with minor changes in duration to minimize sample degradation. BALB/c female urine was diluted 1:1 in 0.25 M sodium acetate buffer (pH adjusted at 37 °C) and 1000 Units per mL urine H1 sulfatase extracted from H. pometia (Sigma Aldrich) was added to the first dilatation. Both sulfatase and control reactions were incubated for 2 hours at 37 °C. In order to prepare the treated samples for physiology and mass spectroscopy, we ran the reactions over a Phenomenex Strat-X polymeric reverse phase chromatography column. Columns were washed with 1 volume methanol and 1 volume H_2O before the buffered reactions were applied. After applying reactions to the column, the resin was washed with one volume water/methanol/acetic acid mixture at a 78:20:2 ratio. One column volume of methanol was then used to extract soluble compounds from the resin and these were dried under nitrogen gas. Samples were subsequently dissolved in 1:2000 methanol to their original urine volume in order to match the methanol volume in sulfated steroid stimuli. Mass spectrometry was utilized to measure the loss of sulfate precursor ions in the sulfatase treated sample compared to the control sample[25]. We observed that compounds in the range of m/z 300 to 350 were lost in the sulfatase treated but not control treated urine.

AOB GCaMP2 Ca^{2+} imaging

Volumetric images of the mouse AOB were acquired from *ex vivo* preparations inside the custom tissue imaging chamber using an objective-coupled planar illumination (OCPI) microscope[24]. The microscope consists of a 20x water immersion objective (Olympus, Center Valley, PA, USA) mounted on a piezoelectric objective actuator (Piezosystem Jena, Hopedale, MA, USA). A custom-designed coupler linked an optical fiber, a light collimator, and a light sheet-forming cylindrical lens oriented at 90° to the focal plane of the microscope objective. Images were taken using a 1004×1002 pixel EM-CCD camera (Andor, South Windsor, CT, USA) located after a 100 mm tube lens (Infinity Photo-Optical Company, Boulder, CO, USA). Volumetric images were produced by scanning the light sheet across the tissue. The total scan range along the "z" axis was 400 μm, and the "z" step size was typically 8 μm. Voxel dimensions were 0.71 μm × 0.71 μm × 8 μm, and thus the total dimensions of image stacks were 713 μm × 712 μm × 400 μm. The total time to acquire and write each image stack to disk was 5s.

Prior to image acquisition, the superfusing aCSF was warmed to 33–35° C. 11 sulfated steroids (1–100 μM), 100-fold diluted BALB/c male and female urine, and control Ringer's stimuli were delivered to the VNO through the polyimide cannula using a pressurized, computer-controlled stimulus delivery system (AutoMate Scientific, Berkeley, CA, USA) or

an UltiMate 3000 analytical autosampler (Dionex, Sunnyvale, CA). Each stimulus lasted approximately 5 image stacks (25 s) and was followed by a recovery period of approximately 10 image stacks (50 s). All stimuli were presented in 3–5 randomized, interleaved blocks. In a small subset of experiments, we acquired images from single frames at 10 Hz, stimulating the VNO for with P8200 or Q1570 for 10 s with a recovery period of 50 s.

Ca^{2+} imaging analysis

Volumetric movies (each ~100 GB in raw form) were analyzed in MATLAB (Mathworks, Natick, MA, USA) using custom software described previously (Turaga and Holy, 2012). Each image stack was "registered" to a reference stack acquired between stimulus presentations near the middle of the experiment. Image registration typically reduced the mean squared difference between the voxels in the stack by ~100 fold.

To measure resting-state fluorescence from GCaMP2 signals, we averaged the fluorescence intensity (*f*) at each image voxel in 3–5 consecutive stacks prior to stimulus onset (f_{rest}). To measure stimulated activity, we averaged the fluorescence during the 3–5 stacks of stimulus presentation to the vomeronasal organ (f_{stim}). From these, we computed the relative change in fluorescence intensity:

$$\frac{\Delta F}{F} = \frac{f_{stim} - f_{rest}}{f_{rest}}$$

To measure the reliability of responses across repeated stimulus presentations, we also computed the "response reliability index" (*RRI*):

$$RRI = \frac{mean(\Delta F / F)}{stdev(\Delta F / F)}$$

where *stdev* represents standard deviation of the mean across all stimulus repetitions. This produced a 5-dimensional (nX × nY × nZ × n_stimuli × 2 metrics) activity matrix. We thresholded 5–D activity matrices, then subjected 4–D maximum projections across stimuli to image flow, wherein each voxel was associated with a nearby peak in $\Delta F/F$ by traversing an "uphill" path of its nearest neighbor voxels. This process produced volumetric ROIs. Some adjacent ROIs shared identical response patterns and no obvious physical discontinuities (i.e. a "split" ROI). We manually merged such ROIs using a customized graphical user interface in MATLAB.

For each volumetric ROI, a scalar response value was produced by weighting the activity of each voxel by its dot product with the mean response, then summing all activity within the ROI. Thus, the Ca^{2+} activity for experiment was condensed to a (nStacks × nROIs) matrix. Only ROIs which responded with $\Delta F/F$ exceeding the various thresholds and which showed statistically significant responses compared to Ringer's controls for at least one stimulus ($p < 0.05$, Wilcoxon rank sum test) were included in subsequent analyses.

For the concentration-response analysis in Supplementary Figure 2, we calculated the GCaMP2 "signal strength", the sum of the Δ*F*/*F* signal for all voxels that crossed experiment-specific *RRI* thresholds. We then normalized these values for each experiment by the maximum value across stimuli and concentrations. Because the maximum value was not always elicited by 100 μM P8200, the average across experiments, even for 100 μM P8200, was less than 100%.

Clustering of glomerular response patterns

From each set of experiments an nStimuli × nROIs matrix of Δ*F*/*F* values was computed as described above. We utilized clustering algorithms (based on mean shift clustering[44]) to identify common patterns of activity in the population (Figs. 3f and 6b). We evaluated sulfated steroids cluster results at multiple ROI thresholds (Supplementary Fig. 5). The resulting patterns strongly agreed with patterns identifying functional classes of VSNs from somatic recordings[27, 31]. For steroid clusters (VSN classes), labels were arranged to match a common numeric assignment (Classes 1–10 plus an unclustered group; Fig. 6b).

Analysis of ROI positions

Several methods were used to compare the positions of ROIs. To measure absolute glomerulus positions (Fig. 4 and Supplementary Fig. 6), we first identified ROIs on the basis of their responses to one or more stimuli. For each experiment, we generated a set of 3 orthogonal vectors indicating the anterior/posterior, medial/lateral, and depth axes using a biplanar fit to the surface of the tissue and the visible division between the aAOB and pAOB (the *linea alba*[45]). We then measured ROI positions along each of these axes by computing the dot product between the ROI position and the orthogonal vectors. We then normalized the ROI positions along each axis. We simplified each ROI as a sphere (matching the centroid and volume of observed ROIs), and then measured the tendency for ROIs of each class to occupy positions along each axis. We did this by normalizing to the total occupancy across all classes, and then comparing these relative occupancies to those expected from 100,000 shuffled glomerular maps. In the shuffle test, ROI positions remained static but cluster identities were scrambled. Shuffle tests were used to indicate the 95th percentile, corresponding to a 95% confidence interval for relative occupancy. Glomerular classes showing preferential occupancy along any axis show relative occupancy exceeding this 95th percentile.

For measurements of relative spacing between glomeruli, (Figs. 4e and 8b), pairwise distances $d_{ROI(1,2)}$ were computed as:

$$d_{ROI(1,2)} = d_{C(1,2)} - \sqrt[3]{\left(\frac{3}{4\pi}\right) V_{g(1,2)}}$$

Where $d_{c(1,2)}$ is the Euclidean distance between ROI centroids and $V_{g(1,2)}$ is the geometric mean of the ROI volumes. In this case, we used a shuffle test (N=10,000) to establish the propensity for randomly-chosen elements in the set to produce a given measured distance. The median minimum pairwise distance from each ROI in Cluster/Class 1 was calculated for

members of all other Clusters/Classes 2–10 (first column of Fig. 4e and 8b). This value was then compared to mean values taken from 10,000 sample sets with the same number of ROIs per class, but with class identities shuffled. We calculated the likelihood of encountering each value by computing a physical spacing index (*PSI*):

$$PSI = \frac{median_{observed} - mean(median_{shuffled})}{stdev(median_{shuffled})}$$

The *PSI* thus resembles the statistical *z*-score. *PSI* values less than 0 indicate values closer together than expected in shuffled sets, and vice-versa.

Chemical space and receptive field analysis

For each sulfated steroid, the chemical structure was entered into online DRAGON software[36, 46], which produced a set of 1,666 of molecular descriptors. Of these descriptors, 1,319 varied across the 11 stimuli. We normalized the values using the formula

$$n_{i,j} = \frac{x_{i,j} - min\,(x_j)}{max(x_j) - min\,(x_j)}$$

Where $x_{i,j}$ represents the raw value of the the i^{th} molecule for the j^{th} descriptor, and $n_{i,j}$ is the normalized value. Thus, the range of normalized values for each descriptor ranged from zero (the minimum observed value for a particular descriptor) to 1 (the maximum observed value for a particular descriptor). We then computed the chemical dissimilarity for each VSN class receptive field pair by calculating the mean Euclidean distances between all components of each class pair. For example, the dissimilarity between Class 1 (responsive to Q1570 and Q3910) and Class 4 (responsive to P3817, P3865, and P8200) was the average Euclidean distance between the 1319-dimensional representations of all steroid comparisons. A pairwise dissimilarity matrix was made, and a 2–D visualization of this matrix calculated using nonclassical multidimensional scaling (MATLAB function “mdscale”; Fig. 7a). This analysis summarizes the differences across all 1,319 chemical descriptors without weighting any particular descriptor as being more or less important for its binding properties. Because the features that relate structure to receptor binding are not clear, this remains one of the best objective ways to compare odorant structures to one another.

We calculated a relative chemical spacing index (Fig. 8c) by comparing pairwise chemical dissimilarity values to 10,000 iterations of a shuffle test. In each instance of the shuffle test, the identity of the steroids giving rise to each receptive field was shuffled (e.g., for Class 4, each of the 3 steroids giving rise to the receptive field was randomly resampled, without replacement within the panel 11 steroids). This process produced values assessing the relative spacing of these receptive fields, with closeness indicated by values < 0 and farness by values > 0. Note that this comparison is specific to the molecules and activity patterns found with this stimulus set.

Isomap and spring embedding analysis

We evaluated the tendency for glomerular juxtaposition and dispersal to be correlated (or anti-correlated) with receptive field similarity using a spring embedding model (Fig. 8d). In this model, normalized estimates of receptive field similarity R_s were used as the spring constant $k_{rf} = R_s^3$. The relative physical spacing between glomeruli was measured using 2-dimensional isomap analysis[47] ("Isomap.m" in MATLAB dimensionality reduction toolbox). To produce the 2D isomap, we identified the 6 nearest-neighbors for each ROI, and measured the probability for members of each other class to be among these neighbors. This produced a matrix of relative juxtapositions J between classes that was symmetrized and normalized (J_{norm}), and then evaluated by isomap analysis. The isomap epsilon term was set to the median value in J_{norm}. The spring embedding model was thus:

$$E=\sum_{i=1}^{n}\sum_{j=1}^{m}k_{rf(i,j)}\,D_{i,j^2}$$

where E is the model energy $k_{rf(i,j)}$, is the receptive field difference between Classes i and j, and $D_{i,j}$ is the pairwise Euclidean distance between the 2D isomap positions of Classes i and j. The observed values for E were compared to 100,000 shuffle test computations of E (E_{sim}) in which the $D_{i,j}$ terms remained constant while $k_{rf(i,j)}$ were scrambled. Values of E significantly lower than E_{sim} (*i.e.* less than the 5th percentile of the shuffle test) would indicate that similarly-tuned glomeruli are preferentially juxtaposed (i.e. chemotopy based on glomerular juxtaposition/dispersal), and E values higher than E_{sim} would indicate anti-chemotopy. The observed value of E in our dataset (7.1) was just slightly higher than E_{sim} (6.8 ± 0.8).

Supplementary Material

Refer to Web version on PubMed Central for supplementary material.

Acknowledgments

Work was funded by the National Institutes of Health, Awards F32DC009352 (JPM), K99/R00DC011780 (JPM), R01DC010381 (TEH), R01NS068409 (TEH), F30DC011673 (GFH), and National Science Foundation IGERT: Cognitive, Computational, and System Neuroscience Award DGE-0548890 (GFH). JPM and DT developed the AOB imaging infrastructure, JPM and GFH conducted the experiments, and JPM, GFH, and TEH analyzed results and wrote the manuscript.

References

1. Marshall WH, Woolsey CN, Bard P. Cortical Representation of Tactile Sensibility as Indicated by Cortical Potentials. Science. 1937; 85:388–390. [PubMed: 17777206]
2. Hubel DH, Wiesel TN. Receptive fields, binocular interaction and functional architecture in the cat's visual cortex. The Journal of physiology. 1962; 160:106–154. [PubMed: 14449617]
3. Merzenich MM, Knight PL, Roth GL. Representation of cochlea within primary auditory cortex in the cat. J Neurophysiol. 1975; 38:231–249. [PubMed: 1092814]
4. Vassar R, et al. Topographic organization of sensory projections to the olfactory bulb. Cell. 1994; 79:981–991. [PubMed: 8001145]

5. Chen X, Gabitto M, Peng Y, Ryba NJ, Zuker CS. A gustotopic map of taste qualities in the mammalian brain. Science. 2011; 333:1262–1266. [PubMed: 21885776]
6. Wachowiak M, Cohen LB. Representation of odorants by receptor neuron input to the mouse olfactory bulb. Neuron. 2001; 32:723–735. [PubMed: 11719211]
7. Ressler KJ, Sullivan SL, Buck LB. Information coding in the olfactory system: evidence for a stereotyped and highly organized epitope map in the olfactory bulb. Cell. 1994; 79:1245–1255. [PubMed: 7528109]
8. Mombaerts P, et al. Visualizing an olfactory sensory map. Cell. 1996; 87:675–686. [PubMed: 8929536]
9. Rubin BD, Katz LC. Optical imaging of odorant representations in the mammalian olfactory bulb. Neuron. 1999; 23:499–511. [PubMed: 10433262]
10. Belluscio L, Katz LC. Symmetry, stereotypy, and topography of odorant representations in mouse olfactory bulbs. The Journal of neuroscience : the official journal of the Society for Neuroscience. 2001; 21:2113–2122. [PubMed: 11245695]
11. Uchida N, Takahashi YK, Tanifuji M, Mori K. Odor maps in the mammalian olfactory bulb: domain organization and odorant structural features. Nature neuroscience. 2000; 3:1035–1043. [PubMed: 11017177]
12. Bozza T, McGann JP, Mombaerts P, Wachowiak M. In vivo imaging of neuronal activity by targeted expression of a genetically encoded probe in the mouse. Neuron. 2004; 42:9–21. [PubMed: 15066261]
13. Johnson BA, Farahbod H, Xu Z, Saber S, Leon M. Local and global chemotopic organization: general features of the glomerular representations of aliphatic odorants differing in carbon number. J Comp Neurol. 2004; 480:234–249. [PubMed: 15514935]
14. Meister M, Bonhoeffer T. Tuning and topography in an odor map on the rat olfactory bulb. The Journal of neuroscience : the official journal of the Society for Neuroscience. 2001; 21:1351–1360. [PubMed: 11160406]
15. Soucy ER, Albeanu DF, Fantana AL, Murthy VN, Meister M. Precision and diversity in an odor map on the olfactory bulb. Nat Neurosci. 2009; 12:210–220. [PubMed: 19151709]
16. Ma L, et al. Distributed representation of chemical features and tunotopic organization of glomeruli in the mouse olfactory bulb. Proceedings of the National Academy of Sciences of the United States of America. 2012; 109:5481–5486. [PubMed: 22431605]
17. Takahashi YK, Kurosaki M, Hirono S, Mori K. Topographic representation of odorant molecular features in the rat olfactory bulb. J Neurophysiol. 2004; 92:2413–2427. [PubMed: 15152015]
18. Murthy VN. Olfactory maps in the brain. Annu Rev Neurosci. 2011; 34:233–258. [PubMed: 21692659]
19. Scalia F, Winans SS. The differential projections of the olfactory bulb and accessory olfactory bulb in mammals. J Comp Neurol. 1975; 161:31–55. [PubMed: 1133226]
20. Belluscio L, Koentges G, Axel R, Dulac C. A map of pheromone receptor activation in the mammalian brain. Cell. 1999; 97:209–220. [PubMed: 10219242]
21. Rodriguez I, Feinstein P, Mombaerts P. Variable patterns of axonal projections of sensory neurons in the mouse vomeronasal system. Cell. 1999; 97:199–208. [PubMed: 10219241]
22. Wagner S, Gresser AL, Torello AT, Dulac C. A multireceptor genetic approach uncovers an ordered integration of VNO sensory inputs in the accessory olfactory bulb. Neuron. 2006; 50:697–709. [PubMed: 16731509]
23. Meeks JP, Holy TE. An ex vivo preparation of the intact mouse vomeronasal organ and accessory olfactory bulb. J Neurosci Methods. 2009; 177:440–447. [PubMed: 19073215]
24. Holekamp TF, Turaga D, Holy TE. Fast three-dimensional fluorescence imaging of activity in neural populations by objective-coupled planar illumination microscopy. Neuron. 2008; 57:661–672. [PubMed: 18341987]
25. Nodari F, et al. Sulfated steroids as natural ligands of mouse pheromone-sensing neurons. J Neurosci. 2008; 28:6407–6418. [PubMed: 18562612]
26. He J, Ma L, Kim S, Nakai J, Yu CR. Encoding gender and individual information in the mouse vomeronasal organ. Science. 2008; 320:535–538. [PubMed: 18436787]

27. Meeks JP, Arnson HA, Holy TE. Representation and transformation of sensory information in the mouse accessory olfactory system. Nature neuroscience. 2010; 13:723–730. [PubMed: 20453853]
28. Hendrickson RC, Krauthamer S, Essenberg JM, Holy TE. Inhibition shapes sex selectivity in the mouse accessory olfactory bulb. J Neurosci. 2008; 28:12523–12534. [PubMed: 19020044]
29. Del Punta K, Puche A, Adams NC, Rodriguez I, Mombaerts P. A divergent pattern of sensory axonal projections is rendered convergent by second-order neurons in the accessory olfactory bulb. Neuron. 2002; 35:1057–1066. [PubMed: 12354396]
30. Yonekura J, Yokoi M. Conditional genetic labeling of mitral cells of the mouse accessory olfactory bulb to visualize the organization of their apical dendritic tufts. Mol Cell Neurosci. 2008; 37:708–718. [PubMed: 18201899]
31. Turaga D, Holy TE. Organization of vomeronasal sensory coding revealed by fast volumetric calcium imaging. The Journal of neuroscience : the official journal of the Society for Neuroscience. 2012; 32:1612–1621. [PubMed: 22302803]
32. Ames A 3rd, Gurian BS. Electrical Recordings from Isolated Mammalian Retina Mounted as a Membrane. Arch Ophthalmol. 1963; 70:837–841. [PubMed: 14061750]
33. Isogai Y, et al. Molecular organization of vomeronasal chemoreception. Nature. 2011; 478:241–245. [PubMed: 21937988]
34. Arnson HA, Holy TE. Chemosensory burst coding by mouse vomeronasal sensory neurons. J Neurophysiol. 2011; 106:409–420. [PubMed: 21525370]
35. Hsu FF, et al. Structural characterization of sulfated steroids that activate mouse pheromone-sensing neurons. Biochemistry. 2008; 47:14009–14019. [PubMed: 19053227]
36. Haddad R, et al. A metric for odorant comparison. Nature methods. 2008; 5:425–429. [PubMed: 18376403]
37. Luo M, Fee MS, Katz LC. Encoding pheromonal signals in the accessory olfactory bulb of behaving mice. Science. 2003; 299:1196–1201. [PubMed: 12595684]
38. Ben-Shaul Y, Katz LC, Mooney R, Dulac C. In vivo vomeronasal stimulation reveals sensory encoding of conspecific and allospecific cues by the mouse accessory olfactory bulb. Proc Natl Acad Sci U S A. 2010
39. Holy TE, Dulac C, Meister M. Responses of vomeronasal neurons to natural stimuli. Science. 2000; 289:1569–1572. [PubMed: 10968796]
40. Dudley CA, Moss RL. Activation of an anatomically distinct subpopulation of accessory olfactory bulb neurons by chemosensory stimulation. Neuroscience. 1999; 91:1549–1556. [PubMed: 10391458]
41. Meeks, JPH.; T, E. Pheromone Signaling: Methods and Protocols. In: Touhara, K., editor. Methods in Molecular Biology. Humana Press; 2013.
42. Ishii T, Mombaerts P. Expression of nonclassical class I major histocompatibility genes defines a tripartite organization of the mouse vomeronasal system. The Journal of neuroscience : the official journal of the Society for Neuroscience. 2008; 28:2332–2341. [PubMed: 18322080]
43. Meeks JP, Holy TE. Electrical recordings from the accessory olfactory bulb in VNO-AOB ex vivo preparations. Methods Mol Biol. 2013; 1068:237–246. [PubMed: 24014366]
44. Comaniciu D, Meer P. Mean shift: A robust approach toward feature space analysis. IEEE Transactions on Pattern Analysis and Machine Intelligence. 2002; 24:603–619.
45. Larriva-Sahd J. The accessory olfactory bulb in the adult rat: a cytological study of its cell types, neuropil, neuronal modules, and interactions with the main olfactory system. J Comp Neurol. 2008; 510:309–350. [PubMed: 18634021]
46. Tetko IV, et al. Virtual computational chemistry laboratory--design and description. J Comput Aided Mol Des. 2005; 19:453–463. [PubMed: 16231203]
47. Tenenbaum JB, de Silva V, Langford JC. A global geometric framework for nonlinear dimensionality reduction. Science. 2000; 290:2319–2323. [PubMed: 11125149]

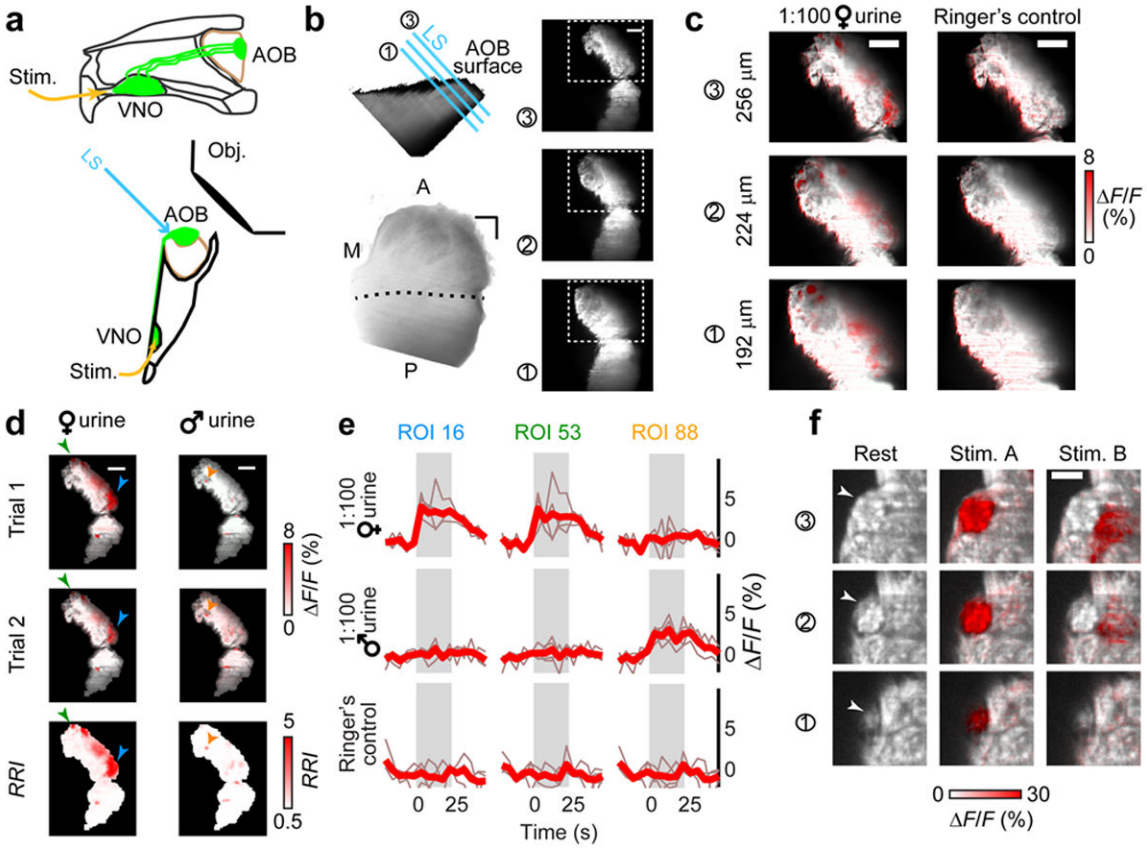

Figure 1. Functional presynaptic Ca^{2+} imaging in the AOB

(a) Midline (top) and ventral (bottom) schematic of the OCPI imaging setup for *ex vivo* preparations. VSNs and their axons are highlighted in green. LS: light sheet used to excite fluorescence. Obj: microscope objective. **(b)** Top-left: side-view of AOB glomerular layer. Cyan lines illustrate 3 positions of the light sheet. Right: images at three light sheet positions. Bottom-left: 3D rendering of the AOB, as seen from the surface. M, A, P: medial, anterior, posterior. Dashed line indicates the *linea alba*, the visible division between the aAOB and pAOB. **(c)** GCaMP2 fluorescence changes during VNO stimulation with dilute BALB/c female urine at the light sheet positions indicated in **b**. **(d)** Glomerular ROIs were defined based on Δ*F/F* intensity and response reliability index (*RRI*), a measurement of the across-trial signal/noise. Δ*F/F* responses to 1:100 BALB/c female (left) and male (right) mouse urine are shown for two different trials (top 2 rows). The *RRI* across 5 trials is shown in the bottom row. Arrowheads indicate the ROIs evaluated in **e**. **(e)** Fluorescence in 3D glomerular ROIs was evaluated during peri-stimulus image stacks and compared to the response to Ringer's control saline. The stimulus timing is indicated by gray shading. Thin traces: individual trials, bold traces: across-trial mean. **(f)** Glomerular boundaries (arrowheads) were evident in the GCaMP2 baseline fluorescence in certain image frames (left). Stimulus-responsive voxels often followed visible anatomical boundaries (middle, 10 µM epipregnanolone sulfate). Nearby voxels activated by other stimuli (right, 10 µM 5-androsten-3β, 17β-diol disulfate) did not cross visible glomerular boundaries. Images

represent mean Δ*F/F* across 4 trials. Three adjacent optical sections are shown. Scale bars: **b–d**, 100 μm; **f**, 20 μm.

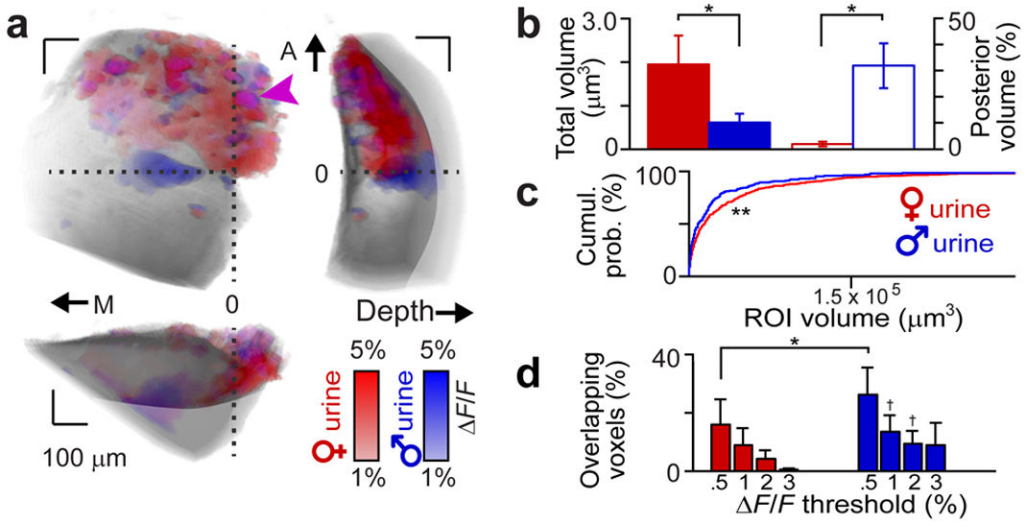

Figure 2. Overlap and distribution of adult BALB/c male and female urine activity maps

(a) Glomerular activity maps to VNO stimulation with BALB/c adult male or female urine. Biplanar fits were made between the *linea alba* and the AOB surface to establish orthogonal (medial/lateral, anterior/posterior, and depth) axes. A reference point was chosen along the *linea alba* at its intersection with the AOB lateral edge (horizontal dashed line). Blue voxels show male urine responses, red voxels show female urine responses, and magenta colored voxels (arrowhead) show glomeruli responding to both. M, A: medial, anterior. 0: reference position. Voxels lying below the horizontal dotted line are considered to be in the pAOB. **(b)** Total volume (filled bars, left ordinate) and fraction of voxels in the pAOB (open bars, right ordinate) of female (red) and male (blue) urine-responsive voxels. **(c)** Cumulative probability histogram of the volume of female (red line) and male (blue line) urine-responsive ROIs. **(d)** Overlap between male and female glomerular response maps across Δ*F/F* thresholds. * and † reflect $p < 0.05$ and $p < 0.1$, respectively (paired Student's *t*-test between male and female). ** reflects $p < 0.05$ (K-S test, n = 8 animals). Error bars reflect s.e.m.

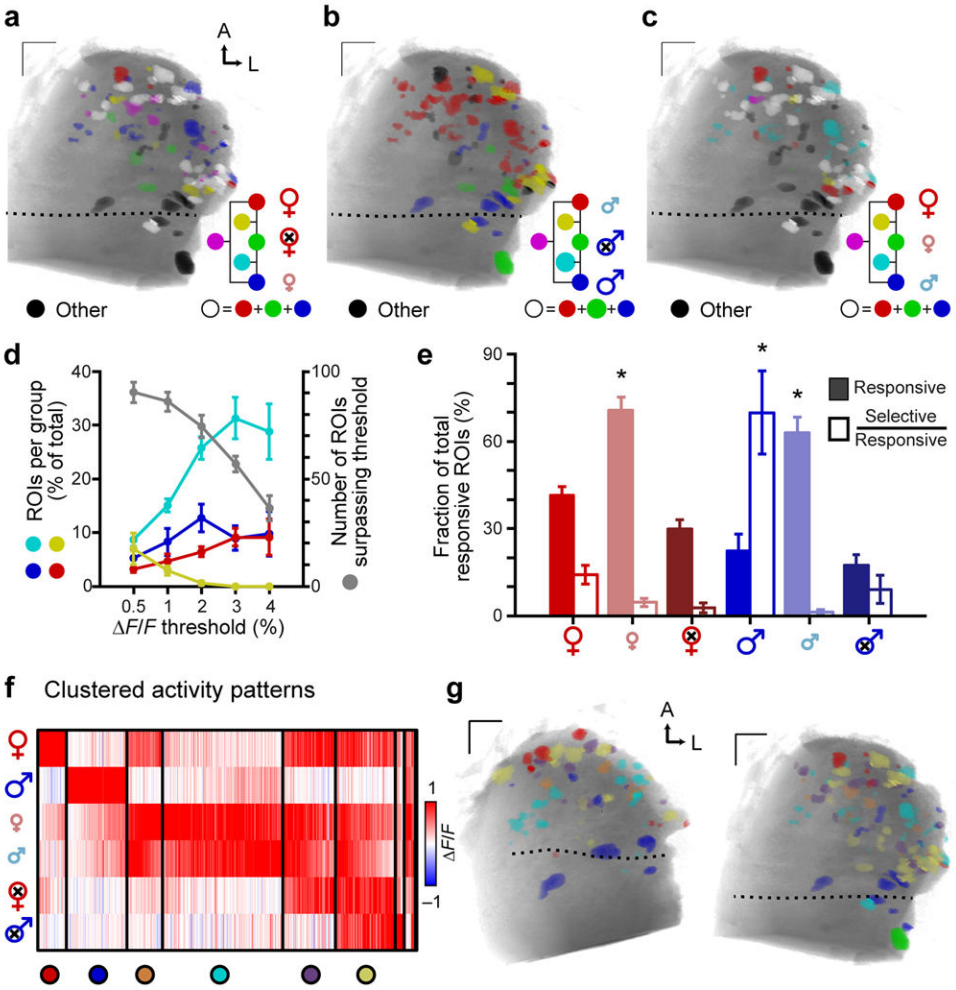

Figure 3. Glomerular maps activated by mouse urine across sex and maturity

(a–c) Example glomerular response maps to dilute BALB/c urine of different sexes and sexual maturities. Colored voxels indicate responsiveness to 3 selected urines in each panel ($\Delta F/F > 2\%$). Color mixtures indicate glomeruli that responded to more than one of the highlighted urines (yellow: red + green, magenta: red + blue, cyan: blue + green, white: all 3). Glomeruli that responded to urine cues other than those highlighted in each panel are colored black. **(d)** Increasing the $\Delta F/F$ threshold reduced the total number of glomeruli (gray symbols, right ordinate), and the prevalence of nonselective glomeruli (yellow symbols, left ordinate). Selectivity for sexually mature female (red symbols), sexually mature male (blue), and juvenile (cyan) urine increased at higher thresholds. **(e)** The percentage of glomerular ROIs responsive (filled bars) and selective (open bars) for BALB/c mouse urine of different sexes and sexual maturities ($\Delta F/F > 2\%$). **(f)** Cluster analysis of glomerular tuning to 6 urines. Each thin vertical stripe shows an individual ROI and rows indicate the stimuli. Vertical black bars divide the clusters. The color of each thin pixel indicates the normalized $\Delta F/F$ for each ROI and stimulus. Colorized circles (bottom) assign unique colors to identify members of each cluster in **g**. **(g)** Functional glomerular maps organized by glomerular tuning. ROI color indicates membership in the associated cluster in **f**. Members of the two

smallest clusters are omitted. Dotted lines indicate the position of the *linea alba*. Scale bars: 100 μm. Error bars represent s.e.m. (n = 5). Asterisks: $p < 0.05$ (one-way ANOVA).

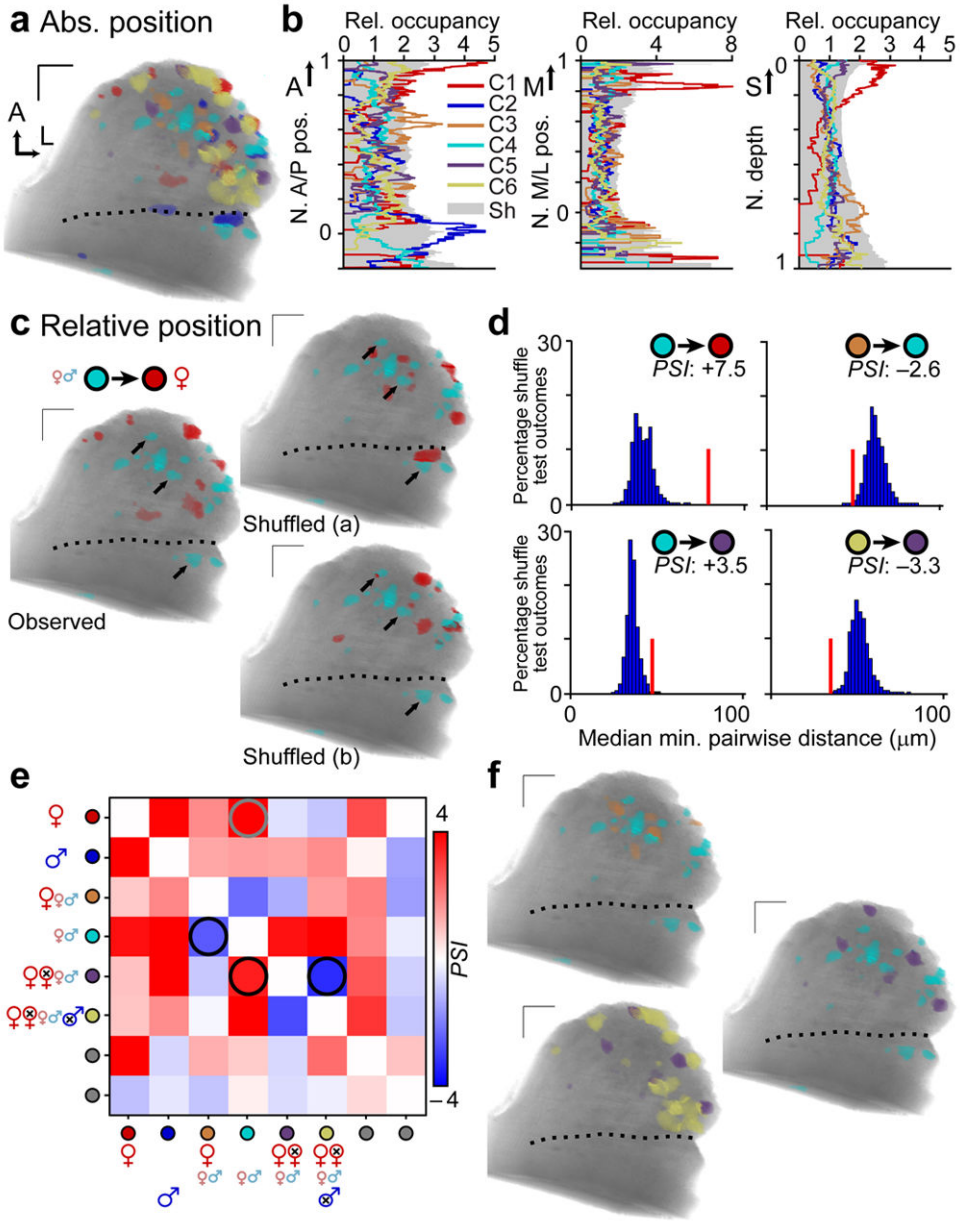

Figure 4. Absolute positions and relative distances between populations of urine-responsive glomeruli

(a) Representative glomerular activity map, with colors assigned as per Fig. 3f. **(b)** Histogram of glomerular positions by cluster along the A/P (left), M/L (middle), and depth (right) axes. The tendency for glomeruli of each cluster to be located at various locations along these axes (relative occupancy) was compared to the 95th percentile from a shuffled map (Sh, gray shading). **(c)** Relative position between glomeruli of Clusters 1 – 6 was likewise compared to expectations from shuffled maps. Black arrows highlight several juvenile-selective glomeruli (cyan) that are more distant from the nearest sexually mature female urine-responsive glomerulus (red) in the observed case than in the exemplar shuffled cases. **(d)** Histogram of pairwise glomerular distances from shuffle tests (blue filled bars ;

10,000 shuffled comparisons per experiment;n = 5) compared to observed distances (red vertical bar). The colored circles indicate the populations being tested. The physical spacing index (*PSI*) resulting from this test is shown for each comparison. Positive *PSI* values indicate preferential dispersal, while negative values indicate preferential juxtaposition. **(e)** *PSI* matrix for all pairwise comparisons, averaged across 5 separate experiments. Red hues indicate preferential dispersal, while blue hues indicate preferential juxtaposition. The gray circle highlights the comparison shown in **c** and the top-left histogram in **d**. Black circles highlight the three other comparisons in **d** and shown in **f**. **(f)** Glomerular maps highlighting the comparisons indicated by black circles in **e**. Dotted lines indicate the position of the linea alba. A: anterior. M: medial, L: lateral, S: surface. All scale bars: 100 μm.

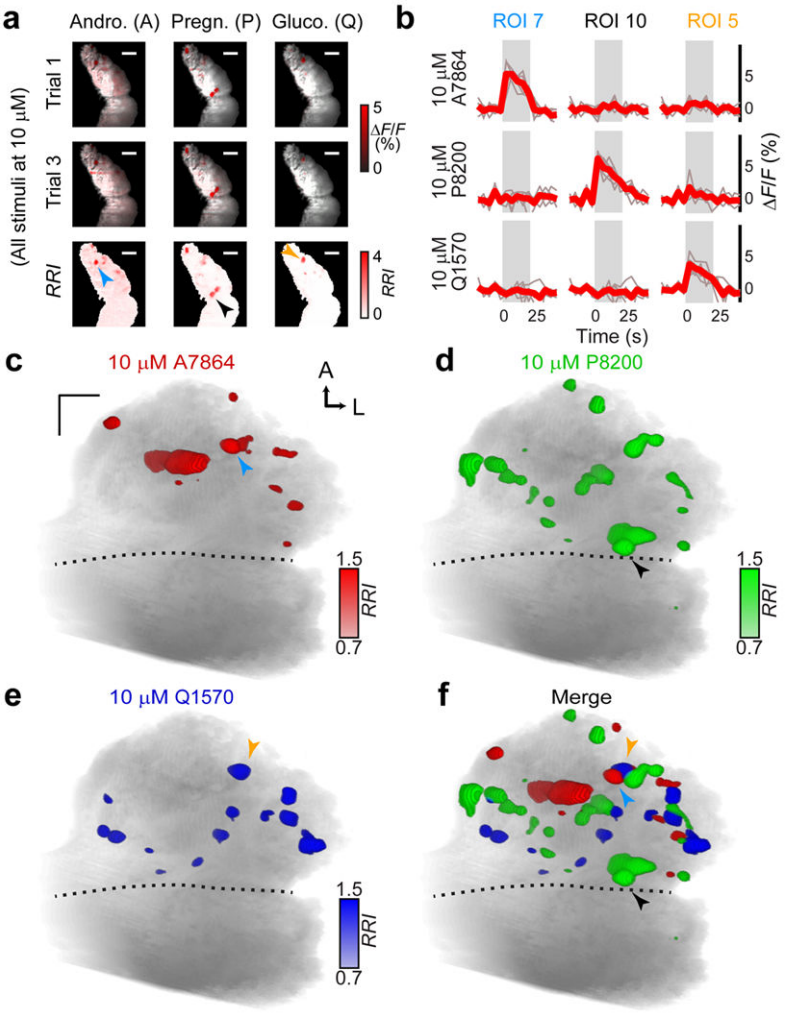

Figure 5. Sulfated steroid VNO stimulation generates robust activity in the aAOB

(a) aAOB glomeruli were activated by VNO stimulation with 10 μM sulfated steroids from different classes (red colored voxels). Two trials per stimulus are presented (top rows) along with the *RRI* (bottom row) for a sulfated androgen (A7864), pregnanolone (P8200), and glucocorticoid (Q1570). Arrowheads in the bottom row indicate glomeruli highlighted in **b – f**. (**b**) ROIs encompassing sulfated steroid-responsive glomeruli were analyzed in the peri-stimulus region (gray rectangle). Thin traces show responses to individual trials, and bold traces represent the average response. (**c**) Activity maps generated by VNO stimulation with 10 μM A7864 were confined to the aAOB. The blue arrowhead marks ROI 7 from **a – b**. (**d–e**) Glomeruli activated by the sulfated pregnanolone P8200 and glucocorticoid (Q1570) were also located predominantly in the aAOB. Black and orange arrowheads mark ROIs 10 and 5 from **a – b**. **(f)** Merged glomerular maps from **c – e**. Scale bars: 100 μm.

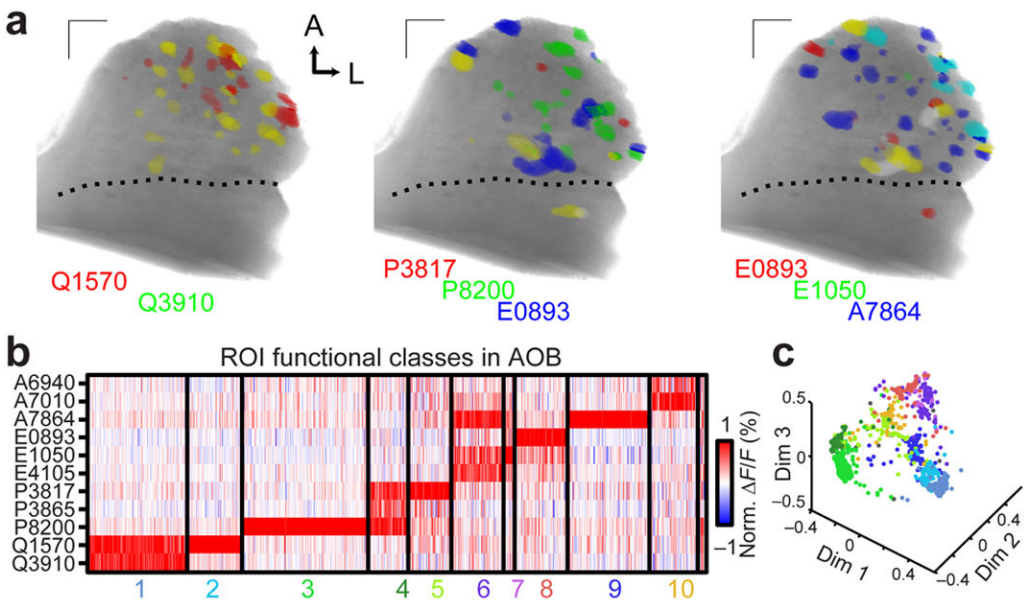

Figure 6. Glomerular activity patterns identify functional VSN classes

(a) Glomeruli responding to the indicated steroids (10 μM) with Δ*F*/*F* > 1% were colorized according to stimulus. Glomeruli responding to more than one steroid are indicated by color mixtures (yellow: red/green, magenta: red/blue, cyan: green/blue, white: red/green/blue). Scale bars: 100 μm. **(b)** 1078 glomerular responses across 10 experiments to the 11-steroid panel match previously-identified VSN functional classes. Each thin vertical stripe shows the activity pattern of a single glomerular ROI, and each row shows responses to a single sulfated steroid (10 μM). A small unclustered group (far right) consisted of less than 1% of all ROIs. **(c)** Multidimensional scaling (first 3 dimensions) of the ROI responses to the 11 sulfated steroids in the stimulus panel. Colors of the points correspond to the clusters in **b**.

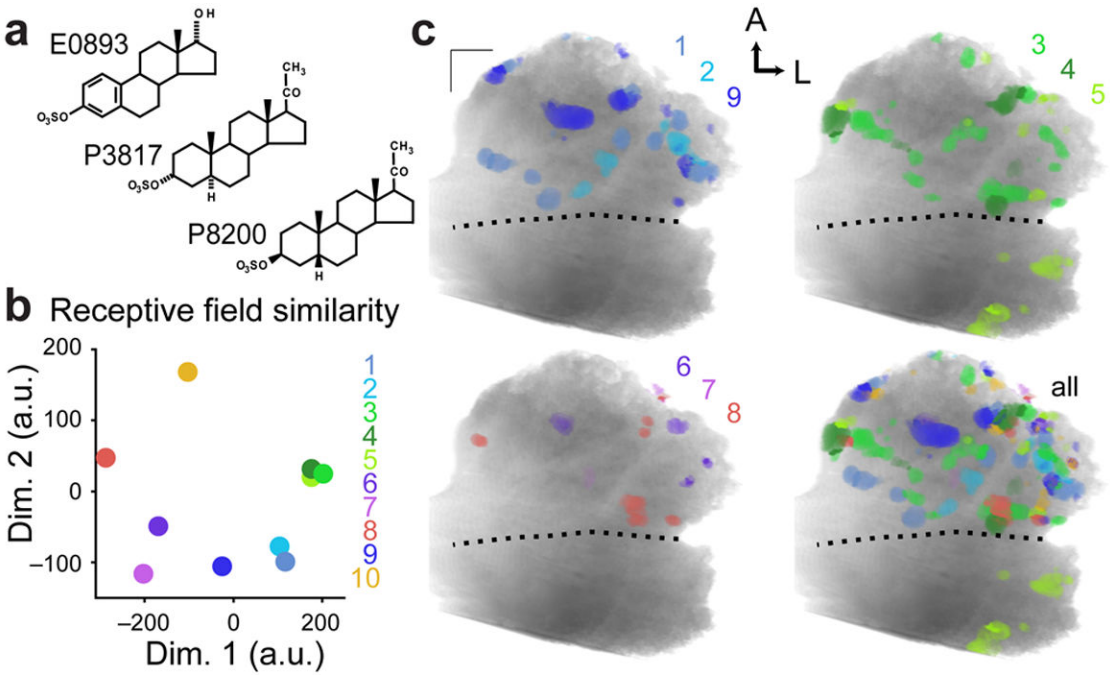

Figure 7. Glomeruli of similarly-tuned VSN classes are distributed across the AOB

(a) Chemical structures for 17α-estradiol sulfate (E0893), allopregnanolone sulfate (P3817), and epipregnanolone sulfate (P8200), 3 of the 11 sulfated steroids in the panel. Responses to these steroids were critical in identifying Class 3 (P8200-dominated responses), Class 4 (responsive to P3817 and P8200), Class 5 (P3817-dominated responses), and Class 8 (E0893-dominated responses). E0893 and P3817 have multiple structural differences while P3817 and P8200 are stereoisomers. **(b)** Relative differences in the receptive fields of each glomerular class were calculated across 1,666 molecular descriptors and displayed here using 2-dimensional nonclassical multidimensional scaling. Symbols for Classes 4 and 5 were shifted slightly from underneath the symbol for Class 3 to allow better visualization. **(c)** Glomerular activity maps for classes with similar receptive fields. Color similarity indicates similar receptive fields, and color opponency indicates disparate receptive fields.

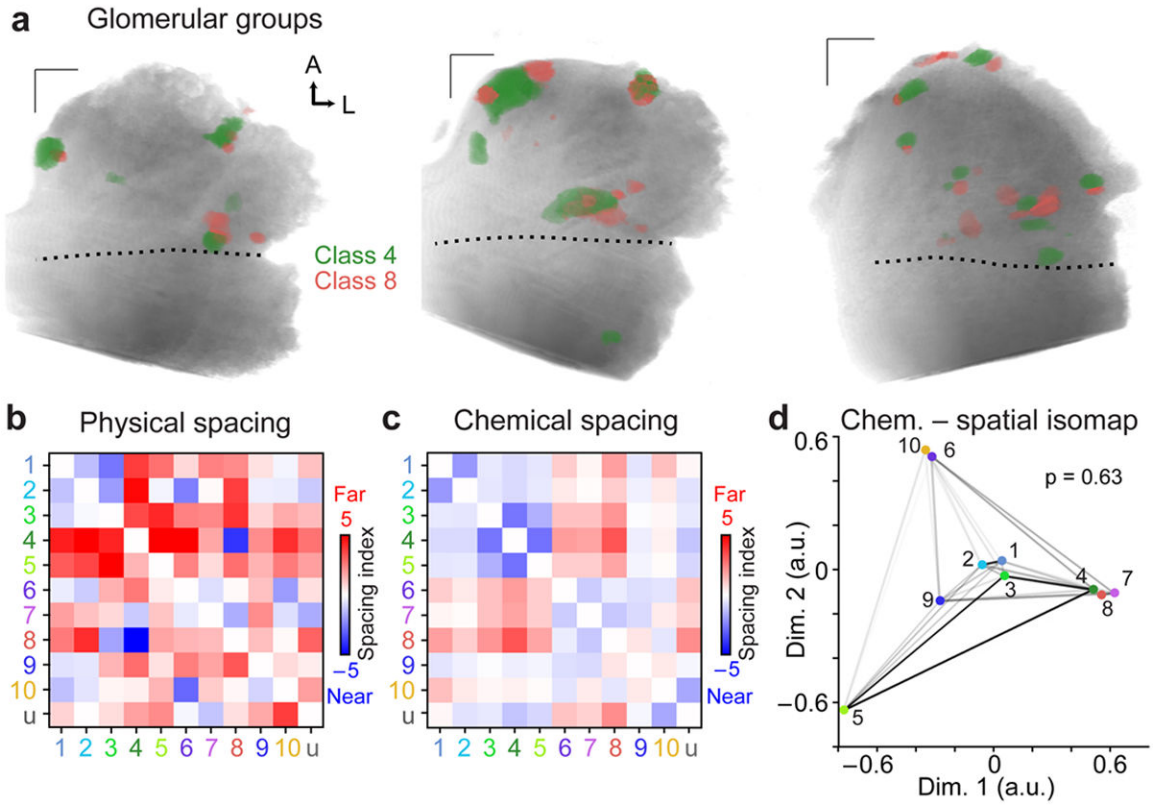

Figure 8. Glomerular juxtaposition does not imply sensitivity to similar odorants

(a) Glomeruli from Class 4, broadly responsive to sulfated pregnanolones, and Class 8, selective for sulfated estradiols, were found in tight proximity in each of ten adult AOBs. **(b)** Physical relative spacing index for all VSN class pairs (n = 10). Blue hues indicate pairs with tight spacing, and red hues those with distant spacing. Elements above the diagonal represent the "forward" test (i.e. from ordinate class to abscissa class) and elements below the diagonal represent the "reverse" test. Group "u" represents the unclustered population from Figure 6b. **(c)** Chemical relative spacing index for all VSN class receptive fields. **(d)** Isomap analysis of physical spacing with receptive field similarity. The closeness of each colored point to others indicates the tendency for that pair to be spatially juxtaposed. The darkness of the shaded connecting lines indicates the similarity of receptive fields, with black representing the most similar and white the most dissimilar. The unclustered group is omitted. The p-value reflects the probability that the observed relationships indicate preferential juxtaposition of similarly-tuned inputs (spring embedding model, 100,000 simulations). A: anterior, L: lateral. Scale bars 100 μm.